MILLIMETER ARRAY
MEMO NO. 84

Possible Phase Calibration Schemes for the MMA

M.A. Holdaway
National Radio Astronomy Observatory
Socorro, NM 87801

June 15, 1992

1 INTRODUCTION

The 225 GHz tipping radiometers which were used in the MMA site survey measured the atmospheric opacity and zenith total power fluctuations (Hogg, 1992). In MMA Memo 68 (Holdaway, 1991), I demonstrated how the phase stability can be estimated from the total power time series taken with the tipping radiometer and reported the raw phase stability (with no calibration) for various atmospheric conditions as a function of time and baseline, in essence, the phase structure function. When the rates of occurance of the various atmospheric conditions are folded into the phase stability estimates, we can estimate how much time the MMA could operate productively at high frequencies in each configuration. It was assumed that rms phase fluctuations of 30° would permit the formation of images with reasonable quality. If the phase fluctuations were less than or equal to 30° over the 1 hour simulation period, phase stable interferometry of very weak objects was possible. If phase fluctuations were greater, then selfcalibration was required. For these cases, only sources which are bright enough to be detected in the time over which 30° phase fluctuations occurred were assumed to be observable.

This method for estimating phase stability from the fluctuations in total power radiated by the atmosphere has not yet been verified against simultaneous direct measurements of the atmospheric phase with an interferometer. A set of approximate structure functions parameterized in the Allan standard deviation is presented for the South Baldy site. We compare our phase structure functions with recent literature, and we find that the South Baldy phase structure function is generally consistent with the results from other phase monitoring programs.

Since there is a need for a better understanding of the relationship between the phase structure function and the resulting images, we simulated the effects of the atmospheric phase errors on images using South Baldy's A configuration. Selfcalibration simulations were also performed.

The relationship between the phase structure function and the structure function of the calibrated phase (ie, the dependence of the residual phase errors upon baseline) is derived and used to analyze a number of different calibration schemes. Among the schemes considered by this document are traditional phase calibration, nutating the subreflector between the calibrator and the target source, simultaneous off-axis calibration, phase extrapolation from low to high frequencies, selfcalibration, and measuring the water vapor column density and determining the atmospheric phase by dead reckoning. Each scheme except the last requires some bright

calibration source to track the atmospheric phase fluctuations. The dead reckoning scheme requires a bright calibrator to track slower fluctuations in atmospheric temperature. It is seen that the calibrator list must include sources down to about 0.15 Jy and the calibrator must be reobserved on timescales of <10 s to be highly effective. Methods for collecting such an extensive calibrator list are discussed.

The Springerville atmosphere is reevaluated in light of the promise some of these phase calibration techniques hold. The differences between the two sites which favored South Baldy for long baseline, high frequency observations in MMA Memo 68 (Holdaway, 1991) are deemphasized by the findings of the current work.

2 FUTURE CONFIRMATION OF METHOD WITH DIRECT PHASE MEASUREMENTS

In the winter of 1988-1989, a number of one hour observations of strong point sources were made with the VLA simultaneously with stability measurements made with the tipping radiometer. The VLA was in its A configuration which has baselines ranging from 1 km to 35 km. Unfortunately, with wind velocities of 12 m/s, the 1 hour radiometer stability measurements are sensitive to atmospheric features ranging from about 100-200 m to about 3-5 km. Hence, the VLA's *direct* phase measurements and the radiometer's *indirect* phase measurements have little overlap in their regime of applicability. When the radiometer data is inverted according to the method presented in MMA Memo 68, the predicted interferometer phases agreed with the VLA phases to no better than a factor of two.

A comparison between direct phase stability measurement and indirect phase stability measurement could be performed with the VLA in its C configuration which has baselines ranging from about 100 m to 3 km. However, the LO is only stable to something like a degree of phase per GHz. To see the atmospheric phase noise above the electronic noise requires very large phase fluctuations which only occur during bad atmospheric conditions. Since we are most interested in the atmospheric conditions with very good phase stability, comparison with VLA data may not be meaningful.

For the last six months of the radiometer's operation on South Baldy, the Smithsonian Astrophysical Observatory's 100 m two element interferometer was directly measuring the atmospheric phase at 12 GHz. The SAO interferometer is sensitive to atmospheric features ranging up to about 100 m. The regime of applicability for the direct and indirect phase stability determination methods have very little overlap. At this time, the Smithsonian data has not been analized.

Some of the work presented here makes the assumption that the rms phase is proportional to baseline raised to the 5/6 power for baselines less than about 150 m, but increase more gently for longer baselines, ie, proportional to baseline raised to the 1/3. This is quite consistent with what is seen in other millimeter and centimeter wavelength atmospheric phase fluctuation studies. Sramek (1990) sees a power law which with a median power of about 0.34. However, most of the data were on baselines much longer than 150 m. When only D array data were

used, and observations dominated by instrumental phase instabilities were excluded, the power law steepened to 0.59, arguing for a change in power law on baselines less than 1000 m. Other observations indicate that there is a steep phase power law for short spacings. For example, the 100 m interferometer on Mauna Kea (Masson, 1991) typically sees power laws of 0.75. The IRAM Interferometer, observing on baselines of 24-288 m, find the average power law to be 0.71. IRAM sees a power law of 0.92 during the day and 0.55 during the night. The steep power law is consistent with what we see on short baselines, Sramek's long baseline power law is consistent with what we see on long baselines, and the IRAM nighttime result is consistent with what we see during the very best conditions, which are likely at night. Keep in mind that in all of these studies there is a fair amount of scatter in the power law exponents, and that the average power law represent a trend.

Both the SMA and IRAM are measuring phase stability on the steep part of the structure function. However, they are extrapolating the steep power law to longer baselines to estimate the utility of future long baseline, high frequency expansions of their arrays. If the phase fluctuations increase less steeply with baseline for longer baselines, then these phase stability estimates are unnecessarily pessimistic.

2.1 PARAMETERIZED PHASE STRUCTURE FUNCTION

Some of the calculations in the following sections estimate the calibrated phase in terms of the phase structure function at some baseline relevant to the calibration process. (The phase structure function is defined as the variance of the phase over long times as a function of baseline, so the RMS phase error is the square root of the phase structure function.) The calculation of the relevant baseline is independent of the model used for the atmosphere and the phase structure function. However, to convert this baseline into an RMS phase error (after calibration), we must know the phase structure function. For this reason, we present the model phase structure functions for South Baldy in terms of the Allan Standard Deviation at 56 s (ASD_{56}). For $ASD_{56} \leq 0.07$, the phase structure function is given by

$$D_\phi(\rho) = \left(8.3 ASD_{56} \rho^{0.54}\right)^2, \tag{1}$$

where ρ is the baseline in meters and the phase deviation is in degrees. For $ASD_{56} > 0.07$, the phase deviation is given by

$$D_\phi(\rho) = \left(4 ASD_{56} \rho^{0.76}\right)^2 \qquad \rho < 150m \tag{2}$$

$$D_\phi(\rho) = \left(28 ASD_{56} \rho^{0.36}\right)^2 \qquad \rho > 150m. \tag{3}$$

These expressions are approximate and are derived from averaging the Allan standard deviations from several stability observations during similar atmospheric conditions (see Holdaway, 1991). In the analysis below, these approximations of the phase structure functions will be used in the short baseline regime (<100 m) where the tipper's uncertainty is high. However, it does not seem unreasonable to extrapolate in this region since this is consistent with the Kolmogorov prediction.

3 A ARRAY SIMULATIONS

Any differential phase errors between the two antennas will result in a phase error in the visibility, which will result in an error in the image. For the simple case of a point source in the image plane, a snapshot of $N(N-1)/2$ visibilities in the (u,v) plane, and small random phase errors of RMS ϕ radians, the *dynamic range* DR (image peak divided by off-source RMS) is estimated by Perley (1989) as

$$DR \approx N/\phi. \tag{4}$$

The MMA design calls for 40 antennas, so a DR of 100 requires the phase errors to be less than 30°. In MMA Memo 68 we used this criteria to define conditions which would permit useful imaging with the MMA.

This naive treatment does not account for the fact that phase errors on short baselines will be less severe than phase errors on longer baselines. It is not straightforward to generalize from a *fictitious* snapshot with uncorrelated Gaussian phase errors to a long integration with phase errors that are coherent over some baseline-dependent time. Finally, this treatment must break down for large phase errors. These complications can be readily dealt with by performing numerical simulations. Our model atmosphere (a 2-D phase screen) is blown over the array, and the simulated visibilities at each time are corrupted by the appropriate gains.

We present in Table 1 the results from a campaign of some simple simulations. A bright point source (no thermal noise) is observed for one hour with South Baldy's current A configuration design (Ge, 1992) at 230 GHz. Observations are performed with four different atmospheric models, looking directly overhead and at 30° elevation. Calibration timescales of both one hour and 60 seconds were used. The simulated data were imaged by Fourier transform and CLEAN deconvolution. The success of the image was gauged by the dynamic range (peak over off-source RMS). The dynamic range is not exactly inversely proportional to the RMS phase error in a given column because the form of the phase structure function changes down the column. The dynamic range is not proportional to the RMS phase error *across* columns because the phase errors will be correlated over long times in the 3600 s column but will be largely uncorrelated in the 60 s column. For example, for zenith observations through the 0.04 K model atmosphere without calibration, the dynamic range and the RMS phase error indicate that in the one hour observation there are ~5 observing intervals with independent phase on a 3000 m baseline. With 60 s calibration intervals, there are ~23 observing intervals with independent phase. The RMS phase error on a representative baseline is not a very good indicator of the potential dynamic range; something else must be specified about the degree of correlation of the phase errors over time and position. Until we get more sophisticated, we will just keep in mind that the phase errors are largely uncorrelated after calibration.

Phase-stable (calibrating once) observations are possible for the 0.04 K and 0.07 K models at zenith and the 0.04 model at 30° elevation. Some sort of calibration will be required for reasonable imaging with worse atmospheric conditions. When simulations are performed with complicated sky brightness distributions, the dynamic range decreases by a factor of about 2.

In addition to decreased DR, the phase fluctuations will artificially "resolve" the source due to loss of coherence on the longest baselines. As the atmospheric conditions deteriorate

	Zenith				30° Elevation			
ASD(56 s), K	3600 s		60 s		3600 s		60 s	
	ϕ	DR	ϕ	DR	ϕ	DR	ϕ	DR
0.04	14°	370	5°	2190	28°	130	10°	720
0.07	26°	180	10°	1150	52°	50	20°	390
0.13	42°	80	19°	500	84°	17	38°	180
0.20	69°	40	31°	240	138°	4	62°	85

Table 1: Dynamic range of simulated point sources viewed with the 3000 m configuration at zenith (one air mass) and 30° elevation (two air masses), with 3600 s calibration time intervals and 60 s calibration time intervals at 230 GHz. The RMS phase error on a 2000 m baseline is also shown.

in our simulations, the integrated flux in the map decreases only by about 15% for the 0.20 K atmosphere, indicating that the loss of coherence on the shortest baselines is not significant. However, the image peak drops by 50% for the 0.20 K atmosphere, indicating that we have reached the seeing limit of the atmosphere.

4 CALIBRATION SCHEMES

The typical observation strategy at existing radio interferometers include the observation of an external calibrator about once every half hour. Antenna slewing rates and on-line computer setup times of existing arrays limit the source/calibrator cycle time to a minimum of a few minutes. At millimeter wavelengths, atmospheric phase errors are a bigger problem and may require more drastic measures. First, we determine the structure function of the calibrated phase analytically and through simulations. Then we apply this relationship to understanding the capabilities of several novel phase calibration schemes.

4.1 STRUCTURE FUNCTION OF THE CALIBRATED PHASE

First, we will analytically determine the structure function of the calibrated phase. Figure 1 illustrates a two element interferometer with baseline ρ alternately observing a target source and a calibrator. The distance between the lines of site to the source and to the calibrator in the atmospheric phase screen is d. We assume frozen-in turbulence and (for now) a velocity of zero. After calibration, the residual atmospheric phase on this baseline will be

$$\phi_{cal}(d,\rho) = (\phi(r) - \phi(r+\rho)) - (\phi(r+d) - \phi(r+\rho+d)). \tag{5}$$

The phase structure function (Tatarski, 1961) is defined by

$$D_\phi(\rho) = \langle(\phi(r+\rho) - \phi(r))^2\rangle, \tag{6}$$

and is expressed in terms of the correlation function as

$$D_\phi(\rho) = 2 - 2\langle\phi(r+\rho)\phi(r)\rangle. \tag{7}$$

The average is an ensemble average which can be approximated by a time average over some time which is large compared to ρ/v, where v is the atmospheric velocity. The RMS residual calibrated phase can be expressed in terms of the phase structure function:

$$\langle\phi^2_{cal}(d,\rho)\rangle = 2\left(D_\phi(\rho) + D_\phi(d) - (D_\phi(\rho+d) + D_\phi(\rho-d))/2\right), \tag{8}$$

or for $\rho \gg d$ we have

$$\langle\phi^2_{cal}(d,\rho)\rangle \approx 2D_\phi(d). \tag{9}$$

The RMS phase error made with such a calibration is then essentially independent of ρ and is equal to $\sqrt{2}$ times the square root of the phase structure function on a baseline of d. A more complicated analysis must be made if the turbulent layer is thick. If the atmosphere is moving with velocity v and the interferometers cycle through the source/calibrator observations in time t, then

$$\langle\phi^2_{cal}(d)\rangle \approx 2D_\phi(vt+d). \tag{10}$$

Of course, v and d are vectors, and adding them as scalars represents the worst case.

Similar arguments can be made for the residual calibrated phase structure function when selfcalibration is used to determine and correct the phase. For selfcalibration, there is no difference in the lines of site between calibrator and source, only the atmosphere velocity and the gain averaging time come into the expression:

$$\langle\phi^2_{cal}(d)\rangle \approx 2D_\phi(vt). \tag{11}$$

4.2 CALIBRATION SIMULATIONS

We can check the above arguments for the structure function of the calibrated phase with our atmospheric simulation machinery and atmospheric models.

Consider observations of a bright point source in which we artificially divide the data up into calibration observation and target source observation. We use the calibration data, recorded every t_{cycle} s, to calibrate the target source data which is taken in between the calibration data. If the atmosphere is moving with velocity v, then atmospheric features larger than vt_{cycle} can be effectively removed from the target source data, while smaller features cannot be removed. Figure 2 illustrates the behavior of the atmospheric phase on a 60 m and a 3000 m baseline with selfcalibration timescales of 3600 s, 60 s, and 7 s. As can be seen, there is still a great deal of short time scale structure in the phases, and the short baseline phases are not improved by the calibration. Figure 3a shows the structure function for the model atmosphere and the structure function for the residual 60 s calibrated phase while Figure 3b shows the residual 7 s calibrated phase. With the 12 m/s wind velocity used in the simulations, calibration is expected to improve the phase for baselines greater than $vt_{cycle} = 720$ m for the 60 s case and

84 m for the 7 s case. For baselines shorter than vt, calibration *corrupts* the phase. A similar argument can be made for an external calibrator. If the distance in the turbulent atmospheric layer between the line-of-sight to the source and the line-of-sight to the calibrator is d, the phase on baselines longer than d can be improved by calibration. So, a calibrator can improve the phase only on baselines longer than $vt_{cycle} + d$. After calibration, the residual phase structure function is almost flat and the level of residual phase errors can be estimated for a particular atmospheric model by the RMS (uncalibrated) phase on baselines of order $vt + d$.

For a classical Kolmogorov phase structure function with phase error proportional to $\rho^{5/6}$ for baselines less than ρ_o and to $\rho^{1/3}$ for baselines more than ρ_o, calibration will improve the phase greatly for $vt + d \ll \rho_o$, but the improvement is mild for $vt + d > \rho_o$ where the phase structure function is fairly flat. It should be noted that Truehoft and Lanyi (1987) indicate that there is not a sharp switch between the steep and flat phase power laws, but rather a continuous change in power law slope. Observationally, a flattening has not been observed, but steep power laws are observed on short baselines and flatter power laws are observed on longer baselines. Since our observations indicate that ρ_o is only about 100-300 m, highly effective calibration requires that the source/calibrator cycle time be $\ll$ 25 s and the distance in the atmosphere be $\ll$ 150 m, or $\ll 15°$ on the sky, for a source at the zenith and a turbulent atmospheric layer 1000 m above the array traveling at 12 m/s.

During the best atmospheric conditions on the candidate sites, the RMS phase error is proportional to $\rho^{1/2}$, and no flattening is seen. Hence, there is no critical baseline beyond which phase improvements from calibration become slight. During these good conditions, which occur about 20% of the time during the winter months on South Baldy, there is no compelling argument for extremely short cycle times or extremely close calibrators. Under these conditions, the magnitude of the atmospheric phase fluctuations are small anyway and frequent calibration will be needed only for low elevation observations.

4.3 FAST CALIBRATION

To optimize phase calibration, the quantity $vt_{cycle} + d$ must be minimized. There is a trade-off between close, weak calibrators (long integration times, short slew times, close by in the atmosphere) and further, strong calibrators (shorter integration times, longer slew times, and further away in the atmosphere). We estimate the value of $vt_{cycle} + d$ for MMA observations. The dependence of $vt_{cycle} + d$ on the minimum calibrator source strength and the antenna slew rate will indicate the optimal values of these parameters. The value of the phase structure function at a baseline of $vt_{cycle} + d$ will indicate the level of phase errors that is possible to achieve using external calibration.

The atmospheric velocity as a function of height has been studied by Schwab (1992). A typical value for v_{atmos} is 12 m/s. If the atmosphere cannot be described as a thin phase screen, then a single value of the velocity will not be valid.

The total cycle time will be

$$t_{cycle} \approx t_{source} + t_{cal} + 2\psi/v_{slew} + 2t_{setup} \tag{12}$$

where t_{cal} is the time spent integrating on the calibrator, t_{source} is the time spent integrating on the target source, ψ is the slew distance in degrees, v_{slew} is the slew rate in degrees per second, and t_{setup} is the time required for the online computers to set up prior to taking data.

We parameterize t_{source} in terms of $X = \frac{t_{cycle}}{t_{cycle}-t_{source}}$, so $t_{cycle} = X(t_{cycle} - t_{source})$. The value adopted for X depends upon how much time the observer is willing to sacrifice to calibration. In our analysis, we consider $X = 1.5$, or $\sqrt{3}$ loss in SNR compared to no time spent on calibration. For many combinations of atmospheric conditions, target sources, and array configurations, the image quality will be limited by atmospheric phase errors rather than SNR if such a scheme is not adopted, so throwing away a large fraction of the time to calibrate actually means gaining some time for high frequency, long baseline observing.

An estimate for t_{cal} can be obtained by considering the required accuracy of the gains. Thermal noise will lead to errors in the *complex* antenna gains of order

$$\sigma_G = \frac{\sigma_V}{S\sqrt{N-3}} \tag{13}$$

where σ_V is the noise for a single visibility, N is the number of antennas in the array and S is the calibrator strength (Cornwell, 1989). For high SNR, the gain phases have a Gaussian distribution with RMS of $\sigma_G/\sqrt{2}$ radians (Thompson, Moran, and Swenson, 1986). We assume a Gaussian distribution in spite of the low SNR. Then the RMS error in the gain phase varies as $\sigma_\phi = 6°/R$, where R is the SNR per baseline. We assume here that $R = 1$, as 6° phase errors yeild a DR of 500-1000:1. If higher DR is required, then selfcalibration is probably possible.

For the MMA, the noise per baseline (two Stokes, one IF) will be

$$\sigma_V = 0.001\frac{T_{sys}(\nu)}{\epsilon_a(\nu)\sqrt{t}} \tag{14}$$

where ϵ_a is the aperture efficiency and t is the observing time in seconds and $T_{sys} = T_{rec}+T_{atmos}$, and $T_{atmos} = T_{sky}(1 - e^{-\tau/\sin(\theta)})$, where θ is the elevation angle and T_{sky} is the physical temperature of the air in the moist turbulent layer. We assume everywhere that we can use one IF at a continuum bandwidth of 1 GHz for calibration (or selfcalibration), that T_{rec} is equal to the frequency in GHz (Hjellming, 1989), and that the optical depth τ_ν is related to the column density of precipitable water vapor via $\tau_\nu = A_\nu w$, where w is millimeters precipitable water vapor, and A_ν has been read off of Schwab and Hogg's 1 mm opacity figure (1989) and reproduced here in Table 2. Hence, the amount of time required to obtain a signal to noise ratio of R on a source of brightness S is

$$t = \left(\frac{0.001RT_{sys}}{\epsilon_a S}\right)^2 \approx \left(\frac{0.001R(\nu + 253(1 - e^{-A_\nu w/\sin(\theta)}))}{\epsilon_a S}\right)^2 \tag{15}$$

In the case where the antennas slew to the calibrator position, this time is divided by two since both IFs can observe the calibrator.

At λ 3 mm, there are about 200 compact flat spectrum sources in the sky which are 1 Jy or brighter (Kühr et al, 1979). Hence, the average distance, in degrees, from the target source

ν, GHz	A_ν	ϵ_a
30	0.007	0.9
90	0.01	0.8
200	0.05	0.7
340	0.15	0.6
410	0.3	0.5
650	0.6	0.3

Table 2: Frequency dependence of scaling factor A_ν in $\tau_\nu = A_\nu w$, where w is millimeters of precipitable water vapor; and values of ϵ_a, the aperture efficiency, used in the simulations.

to a calibrator of strength S Jy is

$$\psi \approx \frac{\sqrt{\frac{40000}{200S^{-1.5}}}}{2} \approx 7.1S^{0.75} \tag{16}$$

Most of these sources have a sizable flux in milliarcsecond structure, so will be unresolved to the longest baselines of the MMA.

The slew velocity v_{slew} is not yet determined. The VLA antennas slew at about 0.33°/s, and smaller, modern antennas could probably slew faster. However, the problem will be actually accelerating and decelerating in less than a second, and once on the target or calibrator source, pointing with reasonable accuracy. In most cases where fast external calibration would be required, pointing worse than 1″ would be tolerated since the atmospheric phase fluctuations would limit the DR to a lower value than the pointing errors would.

The online system setup time t_{setup} is also not yet determined. Typically, the setup time for arrays is 10-40 seconds. Several concerns push the MMA setup time to very low values:

- Fast external calibration arguments. These arguments are most compelling for long baseline observations.
- Very large mosaics of bright spectral lines; mosaics with several 1000 pointings, each requiring only 10 seconds or so. The setup time should be much less than 10 seconds for efficient use of the array. This applies to the compact configurations.
- The effects of some sorts of pointing errors on mosaic images are reduced if the entire mosaic is scanned over several times. Again, efficient use of the array requires short setup times. This applies to the compact configurations.
- For low declination sources, the beamshape of the compact arrays depends strongly on the hour angle of the observation (Ge, 1992). This implies that the synthesized beam will change over a mosaic image, and flux in the residuals will be inaccurately determined. One way of getting around this problem is to scan through all pointings many times

over a range of hour angle to yeild more similar synthesized beams for each pointing. This will also improve the performance of the computationally inexpensive linear mosaic algorithm, which assumes the (u, v) coverage is identical for all pointings. This applies to the compact configurations.

We assume that $t_{setup} = 1$ s. Altering t_{setup} will not affect the optimal calibrator source strength, but it will affect the value of $vt + d$, and therefore, the achievable calibrated phase.

The relationship between d, the distance in the atmosphere between the lines of sight, and ψ, the distance on the sky between the calibrator and the source, is optimal when the source and the calibrator are at the same elevation:

$$d = h \sin(\psi)/\sin(\theta) \quad (17)$$

$$d = h \sin(7.1S^{0.75})/\sin(\theta) \quad (18)$$

where h is the height of the turbulent layer of water vapor above the array and θ is the elevation angle above the horizon of the source.

Combining the above expressions, we see we must minimize the quantity

$$d + vt = h \sin(7.1S^{0.75})/\sin(\theta) + X v_{atmos} \left(\left(\frac{0.001R(\nu + 253(1 - e^{-A_\nu w/\sin(\theta)}))}{\epsilon_a \sqrt{2} S} \right)^2 + 2(7.1S^{0.75}/v_{slew}) + 2t_{setup} \right) \quad (19)$$

This expression can be analyzed as a function of elevation θ, atmospheric optical depth τ, calibrator strength S, and slew rate v_{slew}. This analysis does not depend upon any assumptions on the form of the phase structure function and indicates that the optimal calibrator flux is around 0.15 Jy. There will be about 3500 calibrators brighter than 0.15 Jy at λ 3 mm, or a calibrator within 2° of the target source.

Figure 4 illustrates the behavior of the left hand side of Equation 20 ($vt + d$) for a range of slew rates and elevation angles. A few trends are apparent:

- there is almost no difference between the zenith and 60° elevation curves, and little difference between these two curves and the 30° elevation curve. Things fall apart at very low elevation.
- the optimal calibrator flux (ie, the calibrator flux which minimizes the curves) increases as elevation angle decreases (as the atmosphere becomes more important).
- the curves become flatter with higher slewing rates, indicating that less is gained by compiling a calibrator list complete down to the optimal calibrator flux. The curve for 10° elevation is still fairly steep.

The quantity $vt + d$ has been studied as a function of optical depth for a range of elevations angles and source strength, and the main trends are:

	Zenith		30° Elevation	
ASD(56 s), K	no cal	fast cal	no cal	fast cal
0.04	14°	5.5°	28°	12°
0.07	26°	10°	52°	22°
0.13	42°	25°	84°	54°
0.20	69°	41°	138°	90°
0.30	105°	63°	210°	136°

Table 3: RMS phase in degrees over one hour on 2000 m baselines observing the zenith and at 30° elevation for five atmospheric models. The left phase represents essentially no calibration, and the right phase is what is possible with the fast calibration described in the text.

- the difference between curves at different elevations increases with increasing opacity.
- the optimal calibrator flux increases with increasing opacity, the strongest increase coming from the low elevation curves.

The minimum value of $vt + d$ obtained from Equation 20 can be combined with the atmospheric phase structure function to give an estimate of the best possible calibrated phase for a set of parameters θ, τ, v_{slew}, S. We have calculated the value of $vt + d$ for a variety of atmospheric conditions assuming $v_{slew} = 1°/s$, the appropriate τ for each condition, the optimal value of S, and looking at the zenith as well as 30° elevation. Estimates of the best possible residual phase errors are given in Table 3. For observations near the zenith using fast calibration, all of these atmospheric conditions would permit some sort of useful imaging. After fast phase calibration, the phase errors will not be highly correlated over time, so even 50° phase errors may result in an image with dynamic range greater than 100:1. At 30° elevation, the 0.04-0.13 K conditions will result in reasonable images, and the 0.20 K atmosphere may be used for observations which require ~50:1 dynamic range.

4.3.1 REQUIREMENTS ON THE ARRAY: FAST CALIBRATION

For conventional external calibration to effectively remove the effects of the atmosphere at millimeter wavelengths during all but the best atmospheric conditions, the antennas would have to slew at 1-2°/s, the antennas would have to accelerate and decelerate almost instantaneously, the online computers would have to setup in 1 s or less, and an extensive calibrator list would need to be generated.

4.4 BEAM SWITCHING-PHASE REFERENCING

As determined in Section 4.3, highly effective phase calibration at millimeter wavelengths is only possible when the antennas and online computers are extremely agile. Instead of actually moving the antennas, it might be possible to beam switch[1] to the calibrator, or to design the antenna optics such that the calibrator can be observed at the same time as the target source without moving the antenna. The field of view of the antenna will be between 30 and 100 primary beam widths. From our analysis of the density of calibrators on the sky, we know that we need to travel two degrees or more from the target source to get to a suitable phase calibrator. While nutating the subreflector two degrees will not be possible at 230 Ghz, it *will* be possible to see sources 1-2 degrees off axis at 30 GHz, the lowest proposed frequency for the MMA.

If we are beam switching between the calibrator and the target source, the travel time and setup time terms no longer contribute to the cycle time. The atmospheric opacity and the receivers will be more favorable at 30 GHz. There will likely be more suitable calibrator sources at 30 GHz. A new expression for $vt + d$ for beam switching to a calibrator is:

$$vt + d = X v_{atmos} \left(\frac{0.001(\nu_1/\nu_2)(\nu_2 + 253(1 - e^{-A_{\nu_2} w/\sin(\theta)}))}{\epsilon_a S} \right)^2 + h \sin(10 S^{1.25})/\sin(\theta). \quad (20)$$

If it were possible to observe the phase calibrator and the target source simultaneously through a novel optical design, then the factor X becomes 1 and the cycle time is simply the amount of time required to detect the calibrator. One concern here is that the required accuracy of the gains, and hence the required SNR R per visibility and the required observing time increases if we are to know the gains well enough to extrapolate to higher frequencies. The $(\nu_1/\nu_2)^2$ increase in observing time balances out the improvement due to T_{sys} and ϵ_a being more favorable at low frequencies.

It is clear that this technique is not only much easier to perform than the fast slewing, but it also yeilds better calibrations as the quantity $vt + d$ will be much smaller. Figure 5b illustrates the levels of $vt + d$ which can be achieved with beam switching onto the calibrator.

[1] In the literature, *beam switching* usually refers to the total power technique in which the on-signal and off-signal are differenced to remove the effects of atmospheric emission. In this document, *beam switching* refers exclusively to a new technique in which the subreflector is nutated between source position and calibrator position, but the signals are not differenced; rather, the correlated visibilities are stored as two separate sources and the calibrator visibilities are used to solve for the atmospheric gain phases and amplitudes. If both total power and phase beam switching are required, three different beam positions on the sky will be required.

4.4.1 REQUIREMENTS ON THE ARRAY: BEAM SWITCHING

The array must be able to observe at 30 GHz simultaneously or almost simultaneously with each high frequency (115 GHz, 230 GHz, 345 GHz). The beam switching phase calibration method puts tight constraints on the design of the antenna and subreflector. The antenna must have a fairly wide field of view, and the subreflector must be able to move about 3 degrees quickly ($\ll$ 1 second) and accurately (10 arcseconds). The online control system must handle bizarre switching patterns, such as: CAL(2 degrees; 1 second)::25 times { ON-SOURCE(0 arcminutes; 0.02 seconds)::OFF-SOURCE(2 arcminutes; 0.02 seconds) }. The OFF-SOURCE and ON-SOURCE total power signals would be differenced on-line to remove the atmospheric emission from the total power data. Interferometric data would be taken at all three positions. The on-line system would have to accumulate the visibilities for all three positions and store them separately, and the beam switched total power would have to be stored and tagged with the on and off positions. The pointing for both the ON-SOURCE and OFF-SOURCE positions must meet the 1 arcsecond specification. Other specifications must be determined for things like the off-axis gain. In essence, the beam switching phase calibration scheme represents a paradigm shift in array operation and antenna functionality.

4.5 SIMULTANEOUS PHASE REFERENCING

Selfcalibration is the best way to calibrate the atmospheric phase since the calibrator and target source share the same line of sight and there is no time sharing between the calibrator and the target source. If the source is not bright enough to selfcalibrate on, then the next best way to calibrate the source of interest is to simultaneously phase reference on a nearby calibrator. It may be possible to arrange the antenna optics to allow *simultaneous* observations of a target source at high frequency and a calibrator source 1-2° away at 30 GHz. If simultaneous observations are possible, then the residual phase errors after calibration will be about $\sqrt{2D_\phi(vt+d)}$, where $vt+d$ is now given by

$$vt + d = v_{atmos}\left(\frac{0.001(\nu_1/\nu_2)(\nu_2 + 253(1 - e^{-A_{\nu_2} w/\sin(\theta)}))}{\epsilon_a S}\right)^2 + h\sin(10S^{1.25})/\sin(\theta). \quad (21)$$

This is nearly identical to the beam switching case, but the X term is set to 1 (the total observing time is equal to the calibration time). This represents only a small gain in the phase errors, but a $\sqrt{3}$ gain in SNR, since no time is taken away from the target source to perform the required frequent calibration. The values of $vt + d$ as a function of source strength for several values of elevation angle are illustrated by Figure 5c.

4.6 DIRECTIONAL CALIBRATION

I have shown in Section 4.1 that the residual calibrated phase structure function is a function of $vt+d$, at least for baselines long compared to $vt+d$. Up until now, v and d have been considered to be scalars, which is the worst case. Since v and d are really vectors, it is possible to do significantly better phase calibration by measuring the atmospheric phase of the calibrator upwind or downwind from the target source. A delay in the interpolation of the gains can then be calculated based on the wind velocity and the distance d between the target and calibrator sources' lines of site. Such a method would require accurate real time information about the direction and speed of the winds aloft and the height of the turbulent layer. This method works best if the sky velocity and the slewing speeds are matched (ie, if v = 10 m/s and h = 1000 m, it takes 1.7 s for an atmospheric feature to move 1°, so the antenna slewing and on-line setup time should conspire to take 1.7 s to move the same 1°) or if the beam switching frequency is matched with the wind velocity. This method will be limited by the agreement of the wind direction and the calibrator-source orientation, the accuracy of the wind speed, the validity of the assumption that the atmospheric turbulence is "frozen in", and the validity of the assumption that the turbulent layer is thin and therefore has unique height and wind speed. As the sky rotates or the wind changes directions, a new calibrator with the proper orientation to the target source would need to be chosen for optimal calibration. While this method seems promising, it is a messy enough problem that we probably should not count on any great benefit from it.

4.7 SELFCALIBRATION

Selfcalibration is included here for comparison with the fast calibration and the beam switching techniques. Figure 5d shows vt as a function of the flux in compact components (ie, useful flux for selfcalibration). These curves assume an SNR of 1 on each baselines, which leads to phase errors simply due to thermal noise of 6°. Bright sources for which SNR of 1 is reached over times so short that the atmospheric phase fluctuations are less than 6° will require higher SNR and longer integration. It follows that the curves underestimate vt for real observations of bright objects. Also, there will probably be some range of spacings in the (u, v) plane for which selfcalibration is effective, leading to a loss in sensitivity. Again, the curves underestimate the value of vt.

As with the other methods, selfcalibration requires long integration times for sources which are much weaker than about 150 mJy, and hence results in large values of vt. However, since the calibrator and the target source share the same line of sight, there is no penalty in atmospheric distance or slew time in going to brighter and brighter sources, and the phase structure function does not need to be multiplied by $\sqrt{2}$ to get the residual phase error after calibration.

After one of the external calibration schemes has been used to remove most of the gross atmospheric phase fluctuations, the residual phase fluctuations will be not be highly correlated over time. The phase errors will have a mean of zero, timescales of several seconds, and amplitude depending upon the atmospheric conditions. In cases of very bad phase stability

where the residual phase errors are still greater than a radian, there is probably no hope, and selfcalibration will not improve the situation. For somewhat better atmospheric conditions, the residual phase errors after external calibration will be smaller and selfcalibration may help. However, since the remaining phase errors will be over very short timescales, we may not be able to detect the source in the amount of time which the phase fluctuates an appreciable amount. More work needs to be done on the noise characteristics of images made by selfcalibrating data with these very fast residual phase fluctuations.

4.8 COMPARING CALIBRATION METHODS

A comparison of the curves of $vt + d$ can be found in Figure 5. Using the minimum values of $vt+d$ on these curves, Equation 1 through Equation 3 for the phase structure functions, and the relationships between phase structure function and the residual phase errors, we calculate the expected residual phase errors from fast calibration, beam switching calibration, simultaneous calibration, and selfcalibration. The results for zenith observing are shown in Table 4, and the results for observing at 30° are shown in Table 5. The variations in opacity and Allan standard deviation for the various atmospheric stability conditions have been taken into consideration in calculating $vt + d$. Note that the residual phase errors at an airmass of two are worse than twice the residual phase errors at the zenith. This is because T_{sys} increases for low elevation observations, requiring a longer integration on the calibrator, and the distance in the atmosphere between the lines of sight to the calibrator and the source is larger. Also, note that during the best conditions, the residual atmospheric phase is less than 6° for some methods. In calculating $vt + d$ we assumed that we would need to determine the gain phases to within 6°. For the best cases, the gains from the calibrator must be determined with more accuracy; the minimum residual phase error should probably be around 7°. For some of the worse cases where the residual phase error is 30° or higher, we are determining the gains on the calibrator with too much accuracy. For example, letting the error in the phase gains go to 12° requires that we integrate on the calibrator for one quarter the time used in the calculations. This reduction in time will reduce the residual phase errors, but since the d term is not affected and the phase error is proportional to $vt + d$ raised to some power less than one, this will be about a 25% reduction for phase errors greater than 30° for the methods which do not have any overhead in setting up and slewing.

The rate of occurrence of the various atmospheric conditions (see MMA Memo 68) can be folded into these tables to get an idea of the amount of time the MMA can be used with the various calibration schemes. Using the beam switching phase calibration scheme or the simultaneous scheme, zenith observations could be performed during all atmospheric conditions listed here, or over 50% of the time during the winter months. Observations at 30° elevation could be made about 40-50% of the time, but the dynamic range would dip below 100:1 for the 0.20 K and 0.30 K atmospheric conditions.

ASD(56 s), K	fast	beam switch	simult	selfcal
0.04	5.5°	3.2°	3.0°	1.9°
0.07	10°	5.9°	5.5°	3.6°
0.13	25°	13°	12°	7.6°
0.20	41°	22°	20°	13°
0.30	63°	34°	31°	21°

Table 4: Estimates of the residual phase errors after calibration for the fast calibration scheme, the beam switching calibration scheme, simultaneous calibration, and selfcalibration on a 200 mJy continuum source, all looking at zenith at 230 GHz. If there is more continuum flux, the gain solution interval can decrease and smaller phase errors result.

ASD(56 s), K	fast	beam switch	simult	selfcal
0.04	12°	8.6°	8.0°	4.0°
0.07	22°	16°	15°	7.6°
0.13	54°	40°	36°	17°
0.20	90°	66°	62°	31°
0.30	136°	102°	94°	49°

Table 5: Estimates of the residual phase errors after calibration for the fast calibration scheme, the beam switching calibration scheme, simultaneous calibration, and selfcalibration on a 200 mJy continuum source, at 30° elevation at 230 GHz.

4.9 PHASE BOOT-STRAPPING

Because the very high frequency long baseline work is so demanding, it has been proposed that the atmospheric phase be determined at a lower frequency (either by observing the calibrator at a lower frequency or by selfcalibrating at the low frequency while simultaneously observing at the higher frequency), scaled, and applied to the higher frequency source observations. There are a number of reasons why this is a good idea:

- For some source geometries and emission mechanisms, there will be more flux at lower frequencies, thereby decreasing t_{cal}.
- The receivers have lower system temperatures at lower frequencies, decreasing t_{cal}.
- The phase coherence time is much longer at lower frequencies since the additional atmospheric path length is a smaller fraction of a wavelength.

The last point is not really valid since phase fluctuations which occur on timescales shorter than t_{cycle} (or t_{cal} for selfcalibration) will be lost anyway and the phases must be determined more accurately to be scaled up to the higher frequency.

Phase boot-strapping will be most beneficial when there is a great deal of power in large scale phase fluctuations. During the very best conditions, the $\phi \propto \rho^{1/2}$ phase law indicates that there is relatively more power in large scale fluctuations than in small when compared to the usual Kolmogorov case, and phase boot-strapping may have more success. Also, atmospheric phase fluctuations are not the only cause of phase errors in radio interferometers. Poorly calibrated baselines, fluctuating signal pathlengths, and unstable electronics will cause phase errors which may change smoothly through several turns over timescales large compared to t_{cal}, and a low frequency phase-bootstrapping method will remove such phase errors from high frequency observations.

If phase boot-strapping is used, the time required to detect the source will be reduced by a factor

$$\left(\frac{T_{sys}(\nu_1)}{T_{sys}(\nu_2)}\frac{S(\nu_2)}{S(\nu_1)}\frac{\epsilon_a(\nu_2)}{\epsilon_a(\nu_1)}\right)^2 \tag{22}$$

where ν_1 is the lower (calibration) frequency and ν_2 is the higher (target) frequency, T_{sys} is the system temperature, ϵ_a is the aperture efficiency, and $S(\nu)$ is the source flux at frequency ν. Both spectrum and beam size need to be factored into $S(\nu)$. If the phase boot-strapping is to be used in conjunction with selfcalibration of the continuum signal, the source may be weaker at the lower frequency and any gain must be made up by the improvement in T_{sys}.

If the phase is to be scaled from ν_1 to ν_2, it must be determined with greater precision at ν_1. Instead of a SNR of 1 on each baseline, a SNR of about ν_2/ν_1 will be required. A large contribution to T_{sys} is T_{rec}, and the working assumption is that T_{rec} is proportional to ν. While some speed may be gained from aperture efficiency, source spectrum and structure, and atmospheric opacity changing with frequency, this method does not gain a great deal. More is gained at submillimeter wavelengths, especially at low elevation angles, where the atmosphere has a sizable opacity and $T_{sys}(\nu_2)$ increases more quickly than ν.

4.10 TOTAL POWER MEASUREMENTS FOR PHASE FLUCTUATIONS

At millimeter wavelengths, total power measurements are dominated by emission from atmospheric water vapor. Since the MMA is designed to measure total power and interferometric data simultaneously, the non beam switched total power data could be used to determine the atmospheric phases, assuming that the atmospheric phase is dominated by the water vapor path length difference. Analysis of the South Baldy SMA 100 m interferometer and 230 GHz tipper databases should indicate if and under what conditions the bulk of the atmospheric phase truly is due to inhomogeneously distributed water vapor.

The column density of precipitable water vapor w can be determined from

$$T_B = T_{sky}(1 - e^{-A_\nu w}), \tag{23}$$

where T_{sky} is the physical temperature of the moist turbulent air and A_ν is defined in Table 2. This expression breaks down when the water is in the form of droplets. It is difficult to determine w accurately when the atmosphere is optically thick, but who want to observe then? The atmospheric component of the gain phase is then given by

$$\phi = 2\pi 6.5 w/\lambda. \tag{24}$$

Strong signals from astronomical sources must be removed. An accurate value of the kinetic sky temperature averaged over the height range in which the turbulent water vapor is concentrated could be obtained by comparing the phase determined by this method with the phase determined by observations of a calibrator source. In the optically thin limit, any error in T_{sky} propagates into a phase error of

$$\Delta\phi \simeq 2\pi 6.5 w \Delta T_{sky}/T_{sky} \tag{25}$$

indicating that under typical atmospheric conditions at 230 GHz, an error of 1 K in sky temperature results in a 10° phase error.

Neglecting the phase error due to errors in the sky temperature, the residual calibrated phase errors will be on the order of $\sqrt{D_\phi(vt + D)}$, where t is now the amount of time needed to achieve the required SNR for the atmospheric water vapor, D is the dish diameter. The noise in a single total power measurement will be

$$\sigma_{SD} = \frac{T_{rec}}{\sqrt{\Delta\nu t}}, \tag{26}$$

or using 1 GHz bandwidth and the earlier approximation for T_{rec}, the time required to achieve some noise level σ is

$$t = \left(\frac{\nu_{GHz}}{\sigma}\right)^2 10^{-9}. \tag{27}$$

From Equation 24, we see that the water vapor column density must be determined with an accuracy of 0.003 mm for a 5° phase error in the gain phase at 230 GHz. For optically thin skies, this implies that the noise must be

$$\sigma_{SD} < T_{sky} A_\nu 0.003, \tag{28}$$

which is 0.045 K for 230 GHz ($A_\nu \simeq 0.06$) and $T_{sky} = 253$ K. Plugging into Equation 27, the time required for 5° errors is 0.026 s. Hence, $vt + D = 8.3$ m.

Excluding temperature fluctuations, the atmospheric contribution to the residual phase errors should then be $< 5°$ during the 0.30 K atmospheric conditions, the worst conditions which we consider in this memo. Assuming we have an error budget of about 30° of phase per baseline, we can tolerate temperature fluctuations of almost 3 K. The water vapor weighted average of T_{sky} along the line of sight could be calculated from the structure function of T_{sky}. Under the types of conditions which we consider in this memo, the fluctuations of the average temperature will be less than 3°. However, variations in T_{sky} of a few degrees over tens of meters can occur during midday convective conditions, and these sorts of fluctuations are not well described by the Kolmogorov theory of isotropic homogeneous turbulence and may be highly correlated vertically. During these conditions, the fluctuations in T_{sky} may sometimes be large enough to prevent this phase calibration method from being useful.

To summarize, the potential problems with this "dead reckoning" phase calibration scheme:

- This method is not applicable when an appreciable amount of the water is in the form of water droplets rather than water vapor, as ΔT_B is no longer related to w in a simple way.
- What is the nature of the air temperature fluctuations? During what conditions will the air temperature fluctuations be too large for this calibration method to be effective?
- Under what conditions is the atmospheric phase dominated by water vapor?

Since the temperature fluctuations are not well understood at this point, and the residual phase errors will probably be dominated by temperature fluctuations rather than by the variable atmospheric water vapor, we will not attempt to compare this calibration scheme with the other methods discussed above. This is a promising technique, and more will be written about it when we better understand the sky temperature fluctuations.

4.11 REQUIREMENTS ON CALIBRATORS

For most of the phase calibration schemes discussed above, the sensitivity of the MMA puts a lower limit of about 150 mJy on the strength of the source for which calibration is feasible.

How many calibrator sources are there which are stronger than 150 mJy? We have made very naive arguments based on known point sources at 90 GHz. There may be more 150 mJy sources at 30 GHz. It is possible to identify candidate MMA calibrator sources from flat spectrum objects in Condon's 5 GHz and 1.4 GHz all-sky surveys. Observations of promising fields at 22 GHz with the VLA D and C configurations would provide additional information. Better information on the distribution of sources at 30 GHz would help tighten up the antenna requirements and the estimates of the residual phase errors.

Since there may be on the order of 3500 sources 150 mJy or brighter at 30 GHz, or one source within 1.7° on average, it would not be practical to compile a calibrator list from an all sky survey. Rather, a region of the sky around the target source would need to be surveyed

for calibrators prior to the actual observations. Assume that $(2x)^2$ square degrees must be surveyed. We could first start with each antenna observing an independent field in total power. Sampling at $\lambda/2D$, or 0.032 degrees, requires $7500x^2$ individual pointings. Assuming we need a 5σ detection of our 150 mJy calibrator source, and considering the 2.5-fold increase in sensitivity due to the overlap of the primary beams, each sky position needs to be observed by one antenna for only 0.15 seconds. Using the nutating subreflector, we should be able to scan over the entire field with very little dead time. The entire array of 40 antennas could survey the region of interest in total power in $30x^2$ seconds, or six minutes for a 50 square degree region.

The total power survey local to the target source would presumably reveal a large number of unresolved sources. Each of these could be observed with the MMA in interferometric mode to accurately determine the position, flux, and source structure. Determination of these quantities should take a few seconds. In only ten minutes, the candidate calibrator sources for your big observation next week can be located. This requires an integrated expert system which calibrates the total power data, identifies unresolved sources, determines their approximate positions and fluxes, then reobserves them with the entire interferometer, and repeats the identification step. The characteristics of the candidate calibrators should be stored in a database which could be reaccessed the next time the target source was observed.

5 SPRINGERVILLE REVISITED

MMA Memo 68 (Holdaway, 1991) estimated the raw phase stability at both the South Baldy and the Springerville sites but paid little attention to how the phase could be corrected with clever calibration schemes. The results indicated that South Baldy and Springerville were comparable on short baselines or at low frequencies, but that South Baldy had significantly better phase stability on long baselines at high frequency. This was due to two factors: first, the Springerville phase structure function appeared to steepen on long baselines, leading to much higher phases on the longest baselines; second, there was more time on South Baldy when the Allan Standard Deviation at 56 s was as low as 0.04 K or 0.07 K, the atmospheric conditions during which permit phase stable observations on long baselines.

If the phase calibration techniques which have been explored in this memo can be used, the differences between the South Baldy and Springerville sites are not great. The first factor against Springerville disappears because the residual phase after calibration depends only upon $D_\phi(vt + d)$, and $vt + d$ can be made much smaller than the baseline at which the steepening occurs. The second factor is also not highly significant: the very best atmospheric conditions are not required. The fast calibration, beam switching calibration, and probably the total power phase calibration schemes should work well for the atmospheric model characterized by an Allan Standard Deviation at 56 s averaging time of 0.13 K, and South Baldy has conditions this good or better 33% of the time during the winter months, while Springerville has conditions this good or better 30% of the time during the winter months. However, as reported in MMA Memo 68, pages 4-5, the phase structure function at Springerville does not seem to have a

steep section for very *short* baselines, implying that the calibrated phases on South Baldy will still be somewhat better than the calibrated phases on Springerville.

6 SUMMARY

The estimates of usable high frequency time for each configuration of the MMA given in MMA Memo 68 are somewhat conservative. Simulations of the Baldy A Array with model atmospheres overhead and no active phase correction indicate that the 30° phase error criterion results in almost 200 : 1 DR imaging of a simple point source. The improved dynamic range comes about because the phase errors are not correlated over the entire one hour simulation. But even the 0.20 K model atmosphere permits 40:1 DR imaging of a source near the zenith without active phase correction. When the data can be selfcalibration, the correlated parts of the phase errors drop out and the residuals are largely uncorrelated in time, so the same RMS phase error will result in higher DR. The current work indicates that the large configurations may be used for "medium quality imaging" more of the time than estimated in Tables 3 and 4 of MMA Memo 68. The inability of the RMS phase error to uniquely indicate the resulting image quality requires a new way to represent the severity and nature of phase errors. Something like the Allan variance at different averaging times would be appropriate.

Empirical phase structure functions have been derived from the South Baldy data. It has been found that the residual calibrated phase error is given by $\sqrt{2D_\phi(vt+d)}$. We have measurements for v; d can be estimated based on source counts, the calibrator strength, and geometry; t follows from d, the calibrator strength, and other parameters. An analysis of the standard external calibration scheme indicates that it is not very effective at removing the short timescale atmospheric fluctuations unless the online system setup time is very small (1 s), the antennas can slew very quickly (1°/s), and the calibrator source is nearby (2°). It may not be feasible to get the antennas moving back and forth so quickly, but it may be possible to quickly nutate the subreflector between the calibrator and the target source. The field of view is probably wide enough to do this at 30 GHz. It is not clear that the antennas can actually do this. Such a calibration scheme would place new constraints on the antenna design, such as distance of beam throw, accuracy of beam throw, and a highly programable nutating subreflector.

Phase extrapolation from low to high frequencies does not seem very promising except for very high frequencies. Dead reckoning of the atmospheric phases from total power measurements of the water vapor column density may sometimes be limited by the accuracy to which the temperature of the air aloft is known. A scenario is presented for finding very weak calibrator sources; the MMA could find nearby 150 mJy sources in 5-10 minutes, so it could actually be done just prior to the observations.

7 REFERENCES

1. Cornwell, T.J., 1989, *in 'Synthesis Imaging', Publ, A.S.P., eds. Perley, R.A., Schwab, F.R. and Bridle, A.H.*, 185.

2. Ge, Jinp Ping, 1992, "Further Simulations of (Possible) MMA Configurations", MMA Memo 80.

3. Hjellming, R.M., 1989, "Update of MMA Sensitivity Estimates", MMA Memo 59.

4. Hogg, D.A., 1992, "A Summary of the Data Obtained During the mmA Site Survey", MMA Memo 79.

5. Holdaway, M.A., 1991, "A Millimeter λ Phase Stability Analysis of the South Baldy and Springerville Sites", MMA Memo 68.

6. Kühr, H., et al, 1979, "A Catalogue of Radio Sources", Max-Planck-Institute für Radioastronomie, Preprint No. 55.

7. Masson, C., 1991, SMA Memo.

8. Perley, R.A., 1989, *in 'Synthesis Imaging', Publ, A.S.P., eds. Perley, R.A., Schwab, F.R. and Bridle, A.H.*, p. 291.

9. Olmi, L., and Downes, D., 1992, "Interferometric Measurement of Tropospheric Phase Fluctuations at 86 GHz on Antenna Spacings of 24 m to 288 m", *submitted to A.A.*.

10. Schwab, F.R., and Hogg, D.A., 1989, "Millimeter-Wave Atmospheric Opacity and Transparency Curves", MMA Memo 58.

11. Schwab, F.R., 1992, "Lower Tropospheric Wind Speed Statistics...", MMA Memo 75.

12. Sramek, R.A., 1990, in: Radio Astronomical Seeing, eds. J.E. Baldwin & Wang Shouguan, Pergamon, Oxford, p. 21.

13. Tatarski, V.I., 1961, *Wave Propagation in a Turbulent Medium*, Dover, New York.

14. Thompson, Moran, and Swenson, 1986, *Interferometry and Synthesis in Radio Astronomy*, John Wiley & Sons, New York, p. 259.

15. Treuhoft, R.N., and Lanyi, G.E. 1987, Radio Science, **22**, 2, p. 251.

Figure 1: Schematic diagram of a two element interferometer observing a target source and a calibrator through a thin atmospheric phase screen. ρ is the baseline, ϕ are the atmospheric phases, and d is the distance in the atmosphere between the line of sites to the source and to the calibrator.

Figure 2: Simulated 230 GHz phase time series for 60 m and 3000 m baselines, uncalibrated, calibrated with $t_{cycle} = 60$ s, and calibrated with $t_{cycle} = 7$ s.

Figure 3: Simulated 230 GHz phase structure function of uncalibrated data compared to phase structure function for calibrated data: 60 s calibration cycle time (a) and 7 s calibration cycle time (b). The distance vt_{cycle} is marked in the baseline axis.

Figure 4: The quantity $d + vt_{cycle}$ with fast slewing calibration as a function of calibrator strength for a variety of elevation angles and *slew rates*. $\tau = .1$, $v_{atmos} = 12$ m/s, $X = 1.5$, $t_{setup} = 1$ s, and $\nu = 230$ GHz were assumed.

Figure 5: (a) The quantity $vt + d$ for fast calibration, assuming 1 mm water vapor, 1°/s slewing, and 1 s of setup time. (b) The quantity $vt + d$ with beam switching calibration assuming $X = 1.5$. (c) The quantity $vt + d$ with simultaneous observations of calibrator and target source. (d) The quantity $vt + d$ with selfcalibration.

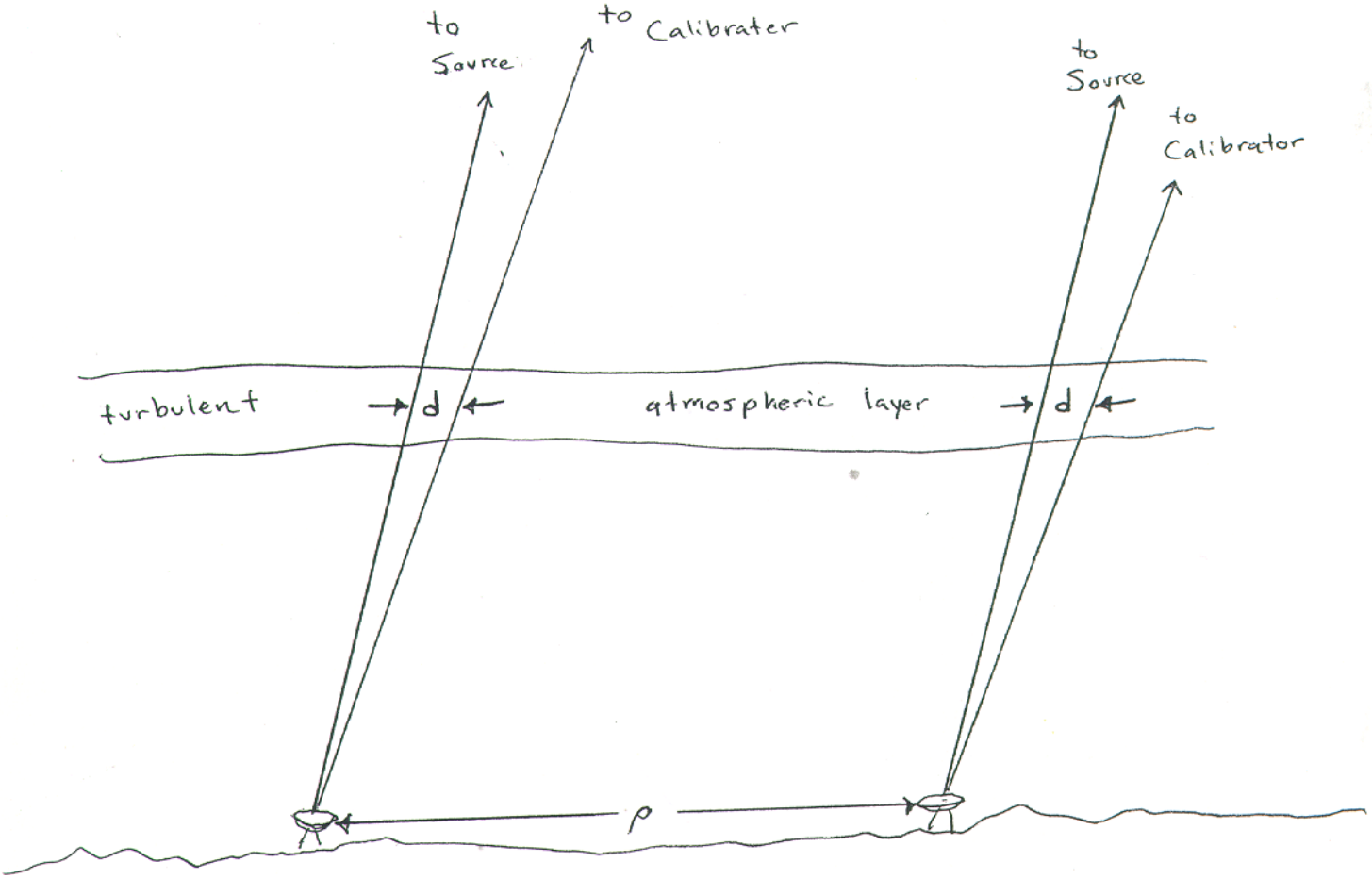

Figure 1

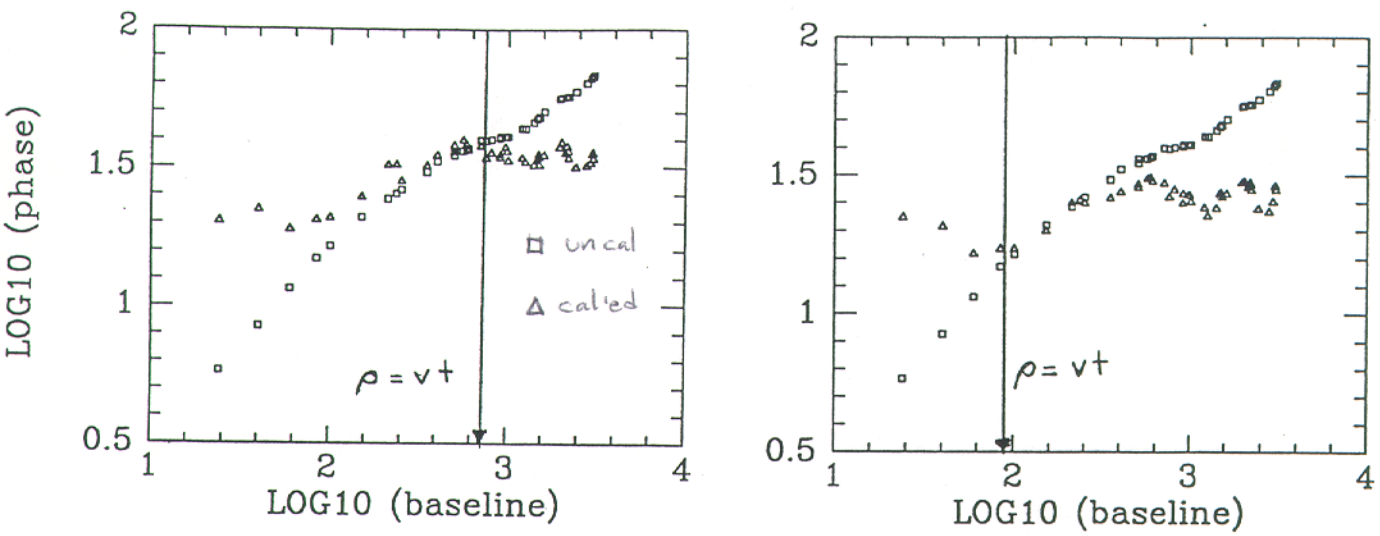

Figure 3: Phase structure function of uncalibrated data compared to phase structure function for calibrated data: 60 s calibration cycle time (a) and 7 s calibration cycle time (b). The distance vt_{cycle} is marked in the baseline axis.

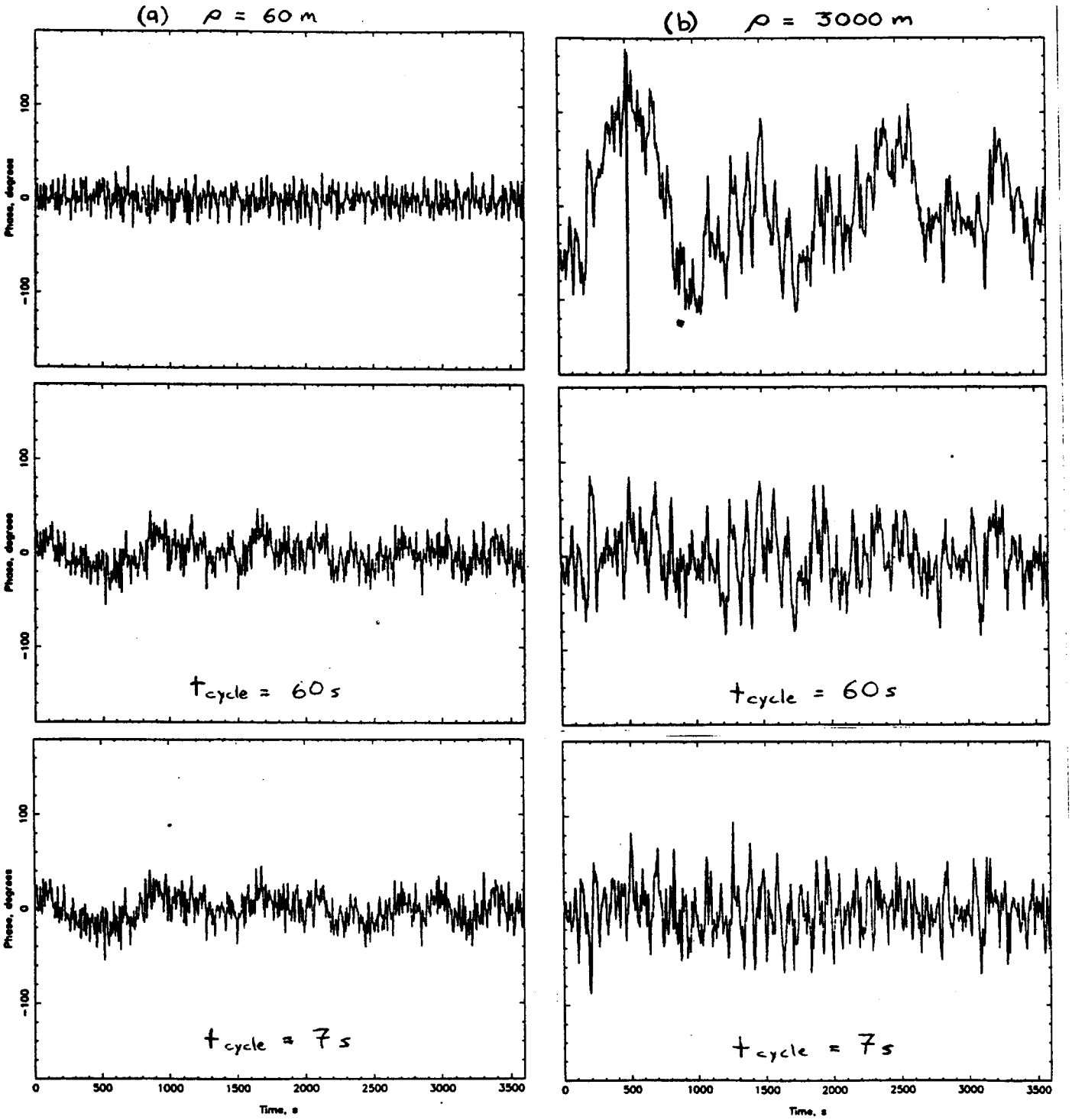

Figure 2: Phase time series for 60 m and 3000 m baselines, uncalibrated, calibrated with 60 s t_{cycle}, and calibrated with 7 s t_{cycle}.

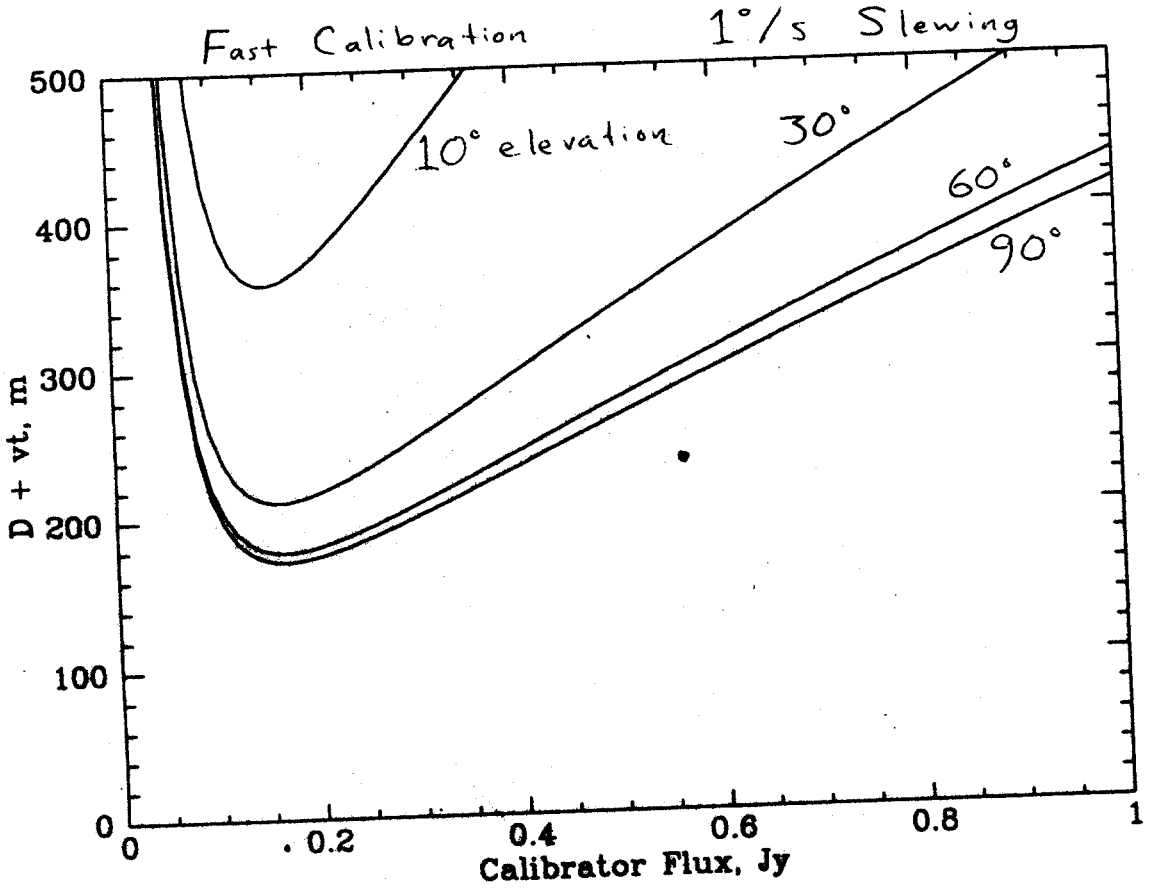
Fast Calibration
1°/s Slewing
10° elevation
30°
60°
90°
D + vt, m
Calibrator Flux, Jy
0
100
200
300
400
500
0.2
0.4
0.6
0.8
1

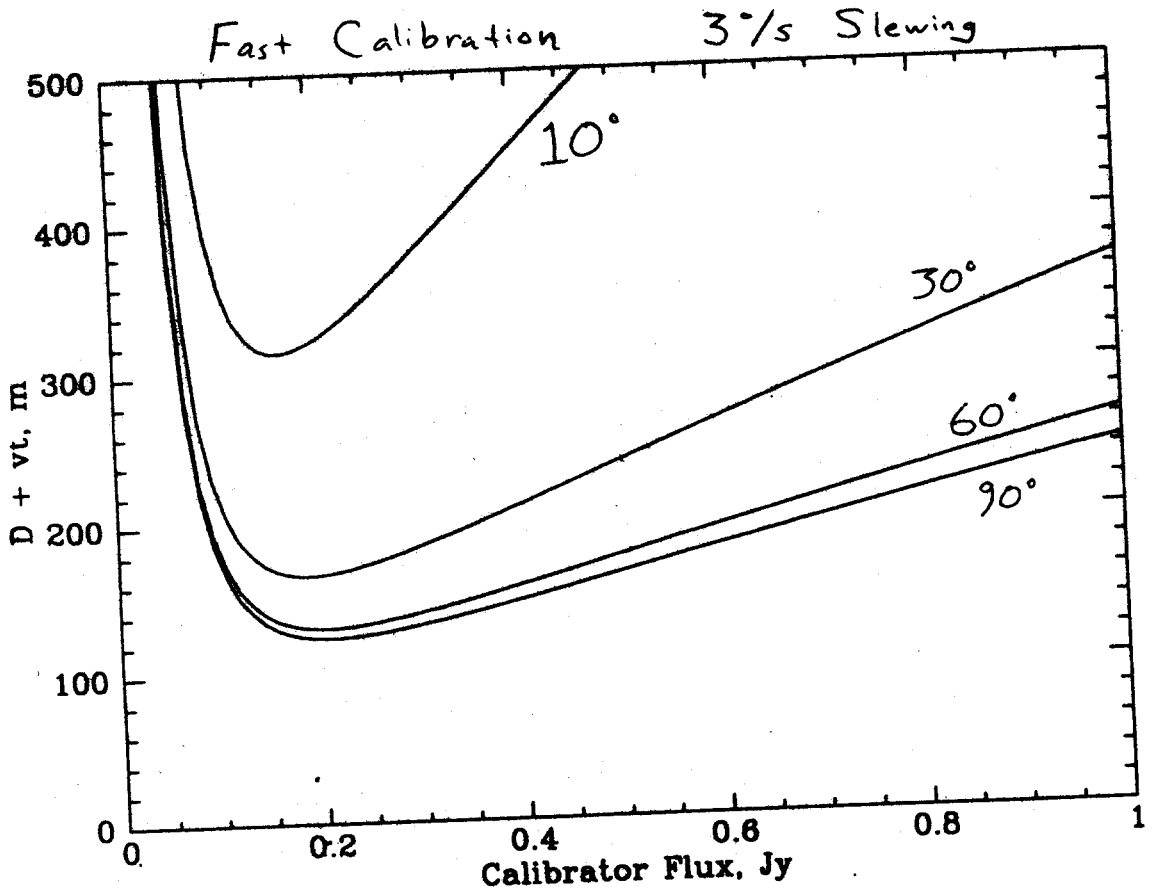
Fast Calibration
3°/s Slewing
10°
30°
60°
90°
D + vt, m
Calibrator Flux, Jy
0
100
200
300
400
500
0.2
0.4
0.6
0.8
1

Figure 4

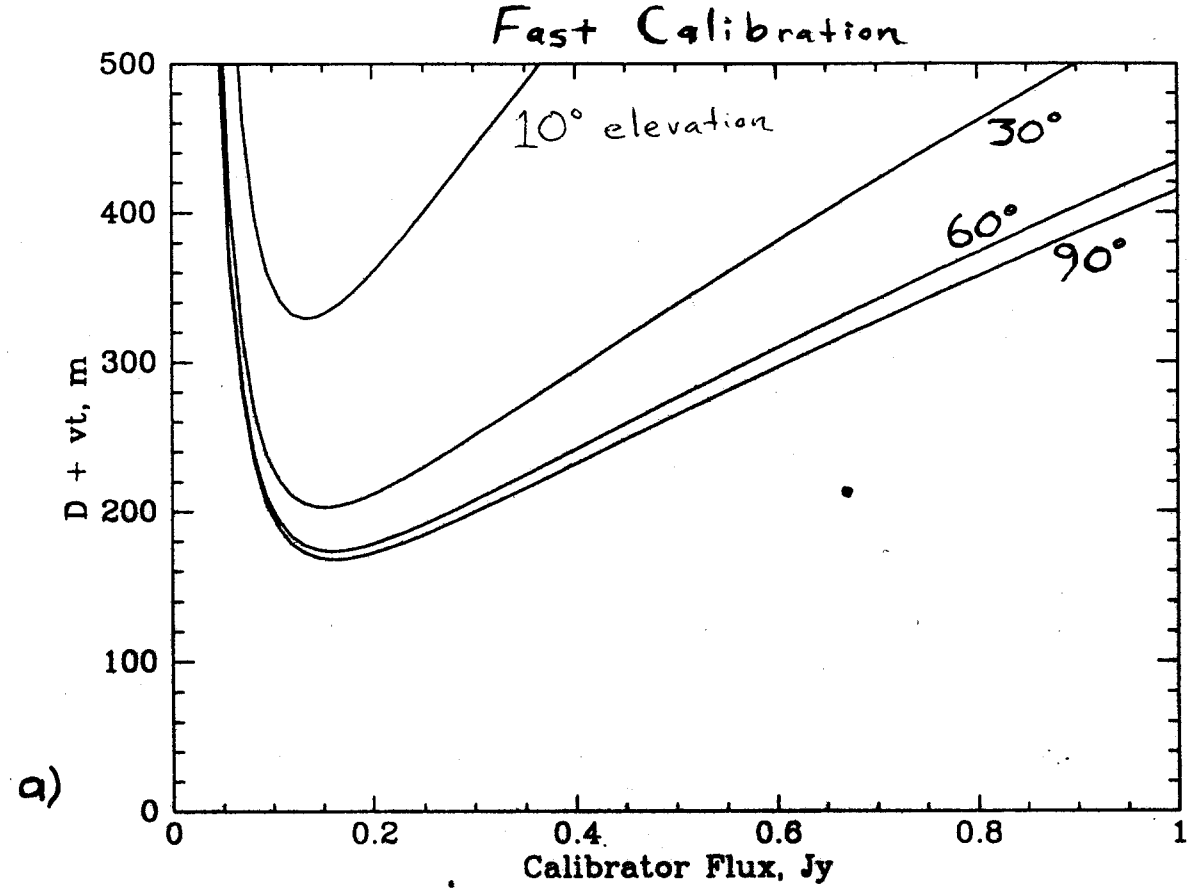
Fast Calibration
10° elevation
30°
60°
90°
D + vt, m
Calibrator Flux, Jy
a)

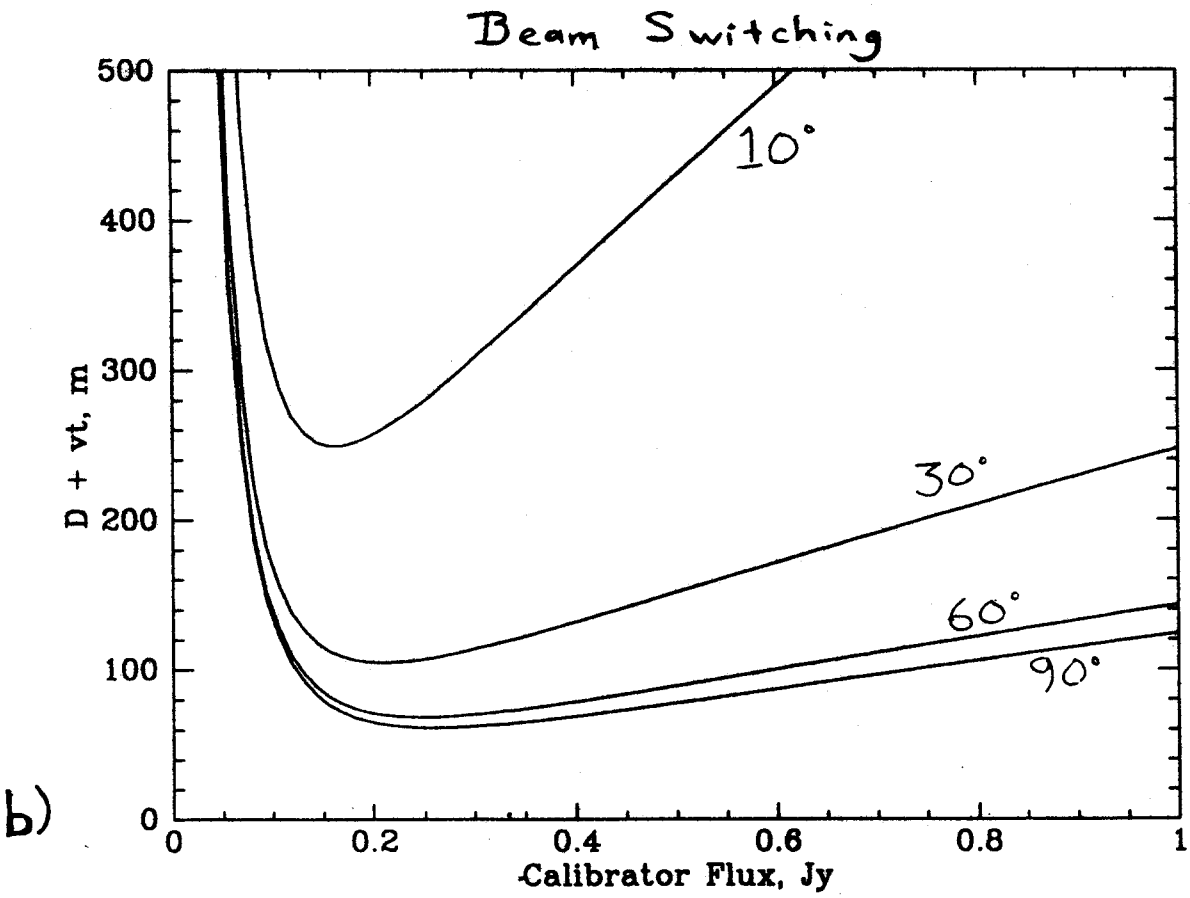
Beam Switching
10°
30°
60°
90°
D + vt, m
Calibrator Flux, Jy
b)

Figure 5

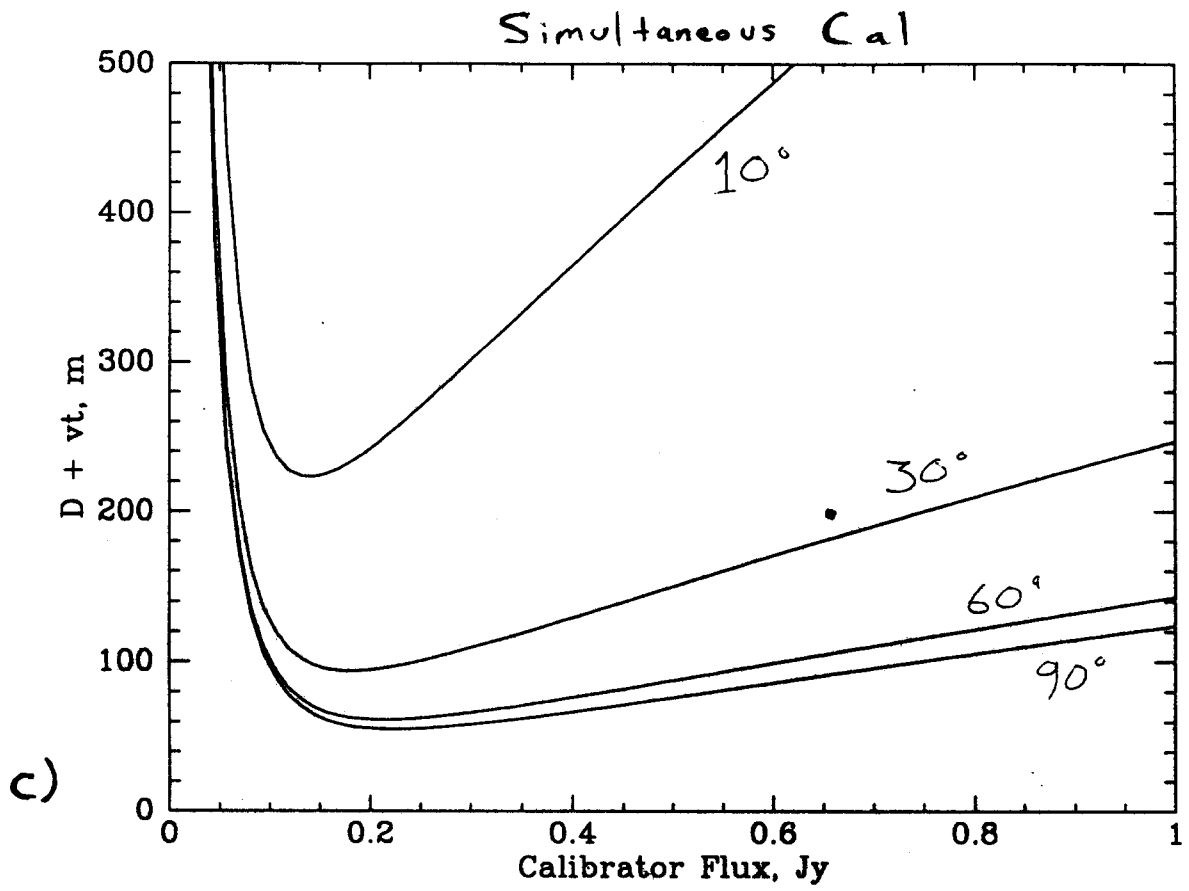
Simultaneous Cal
500
400
300
200
100
0
D + vt, m
10°
30°
60°
90°
0
0.2
0.4
0.6
0.8
1
Calibrator Flux, Jy

c)

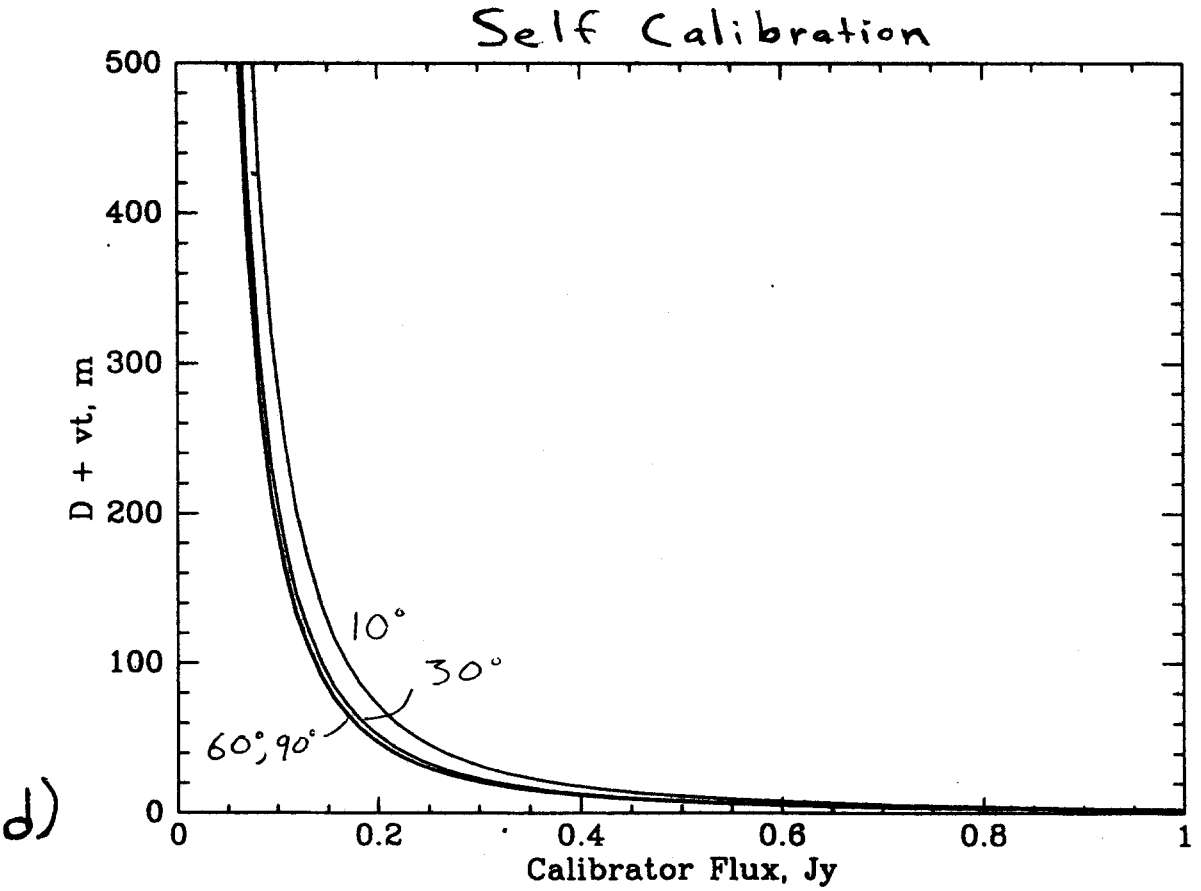
Self Calibration
500
400
300
200
100
0
D + vt, m
10°
30°
60°, 90°
0
0.2
0.4
0.6
0.8
1
Calibrator Flux, Jy

d)

Figure 5